High-Resolution X-Ray Structure of Isoaspartyl Dipeptidase from *Escherichia coli*[†,‡]

James B. Thoden,[§] Ricardo Marti-Arbona,[||] Frank M. Raushel,*[,||] and Hazel M. Holden*[,§]

Department of Biochemistry, University of Wisconsin, Madison, Wisconsin 53706, and Department of Chemistry, P.O. Box 30012, Texas A&M University, College Station, Texas 77842-3012

Received February 10, 2003; Revised Manuscript Received March 3, 2003

ABSTRACT: Isoaspartyl dipeptidase from *Escherichia coli* functions in protein degradation by catalyzing the hydrolysis of β-L-isoaspartyl linkages in dipeptides. The best substrate for the enzyme reported thus far is iso-Asp-Leu. Here we report the X-ray analysis of the enzyme in its resting state and complexed with aspartate to 1.65 and 2.1 Å resolution, respectively. The quaternary structure of the enzyme is octameric and can be aptly described as a tetramer of dimers. Each subunit folds into two distinct domains: the N-terminal region containing eight strands of mixed β-sheet and the C-terminal motif that is dominated by a $(\beta,\alpha)_8$-barrel. A binuclear zinc center is located in each subunit at the C-terminal end of the $(\beta,\alpha)_8$-barrel. Ligands to the binuclear metal center include His 68, His 70, His 201, His 230, and Asp 285. The two zincs are bridged by a carboxylated lysine residue (Lys 162) and a solvent molecule, most likely a hydroxide ion. The product of the reaction, aspartate, binds to the enzyme by displacing the bridging solvent with its side chain functional group. From this investigation it is proposed that the reaction mechanism of the enzyme proceeds through a tetrahedral intermediate and that the bridging solvent attacks the *re* face of the carbonyl carbon of the scissile peptide bond. This structural analysis confirms the placement of isoaspartyl dipeptidase into the urease-related amidohydrolase superfamily.

Peptide bonds in proteins normally occur between the α-carboxylate of one residue and the α-amino group of the following residue. In some instances, however, isoaspartyl peptide bonds have been observed whereby the β-functional group of an aspartate forms a peptide linkage with the α-amino group of the following residue. This isomerization reaction is apparently nonenzymatic in nature and has been proposed to occur via direct nucleophilic attack by the backbone amide nitrogen on the side chain carbonyl carbon of an asparagine residue to form a succinimidyl intermediate (*1*). Subsequent hydrolysis of this intermediate generates either an aspartyl or isoaspartyl peptide bond. The reaction mechanism for the isomerization of an asparaginyl peptide bond is illustrated in Scheme 1. Clearly, the spontaneous introduction of such β-L-isoaspartyl linkages into the polypeptide chain backbone can profoundly effect both protein structure and function.

In *Escherichia coli*, some β-L-isoaspartyl linkages are converted to normal L-aspartyl residues by the enzyme, protein-L-isoaspartate *O*-methyltransferase (*2*). It has been suggested that, in addition to the action of the methyltransferase, a catabolic pathway also exists in *E. coli* to remove β-L-isoaspartyl linkages. The identification of an isoaspartyl

Scheme 1

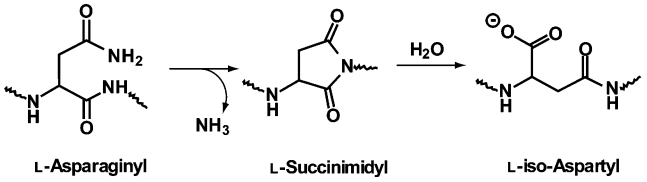

dipeptidase in *E. coli* supports this idea of a degradative pathway (*3*). This enzyme, hereafter referred to as IAD,[1] catalyzes the hydrolysis of β-L-isoaspartyl linkages in dipeptides as outlined in Scheme 2. Interestingly, not all isoaspartyl dipeptides serve as substrates for the enzyme (*3*). For example, Asp-Leu is the best substrate reported to date, followed by Asp-Ser, Asp-Met, and Asp-Val, while Asp-Gly and Asp-His are hydrolyzed at less than 1% of the rate observed for Asp-Leu (*3*). IAD does not catalyze the hydrolysis of tri- or γ-glutamyl peptides (*4*). Recently, isoaspartyl dipeptidase activity has been observed in plant-type asparaginases from *Synechocystis* sp. PCC 6803, *Anabaena* sp. PCC 7120, *Arabidopsis thaliana*, and *E. coli* (*5*).

IAD, cloned and overexpressed from *E. coli*, has a subunit molecular weight of 41 000, corresponding to 390 amino acid residues, and hydrolyzes iso-Asp-Leu with a specific activity of 19 μmoles/min/mg and a K_m value of 0.8 mM (*3*, *4*). The pH-optimum for activity is ∼7.5 (*3*). The role(s) of metal ions and/or cofactors in catalysis is presently not well

[†] This research was supported in part by NIH Grants GM-33894 (to F.M.R.) and GM-55513 (to H.M.H.).

[‡] X-ray coordinates have been deposited in the Research Collaboratory for Structural Bioinformatics, Rutgers University, New Brunswick, NJ, as 1ONW and 1ONX and will be released upon publication.

* To whom correspondence should be addressed. E-mail: Hazel_Holden@biochem.wisc.edu or Raushel@tamu.edu. Phone: 608-262-4988 (H.M.H.) or 979-845-3373 (F.M.R.). Fax: 608-262-1319 (H.M.H.) or 979-845-9452 (F.M.R.).

[§] University of Wisconsin.

[||] Texas A&M University.

[1] Abbreviations: HEPES, *N*-2-hydroxyethylpiperazine-*N*′-2-ethanesulfonic acid; homopipes, homopiperazine-*N*,*N*′-bis-2-ethanesulfonic acid; IAD, isoaspartyl dipeptidase; PMSF, phenylmethylsulfonyl fluoride, SDS−PAGE, sodium dodecyl sulfate−polyacrylamide gel electrophoresis; Tris, 2-amino-2-(hydroxymethyl)-1,3-propanediol.

10.1021/bi034233p CCC: $25.00
Published on Web 04/05/2003

Scheme 2

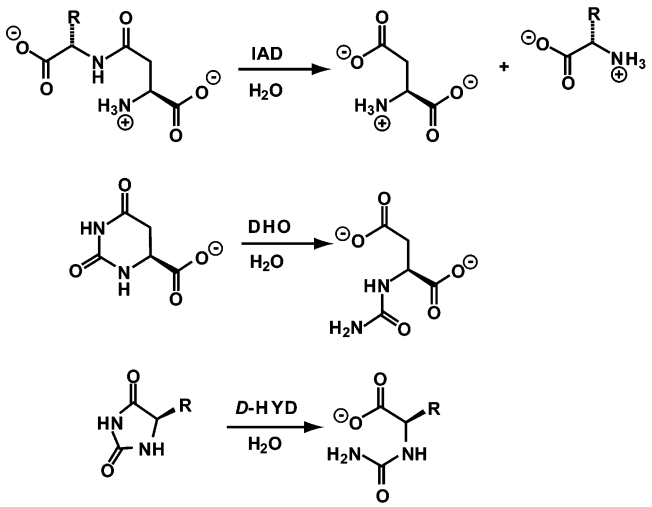

understood. Haley reported that the addition of Mn^{2+}, Co^{2+}, or Zn^{2+} to the purified enzyme was inhibitory, while the addition of EDTA had no effect on the catalytic activity (*3*).

Recent amino acid sequence alignments indicate that IAD most closely resembles dihydroorotase and D-hydantoinase (*4*, *6*). These two enzymes catalyze the hydrolysis of amide bonds within substrates that are remarkably similar to that for IAD, as illustrated in Scheme 2. Both dihydroorotase (DHO) and D-hydantoinase (D-HYD) belong to the urease-related amidohydrolase superfamily (*7*, *8*). The characteristic structural feature of this superfamily is a binuclear metal center that functions to activate a hydrolytic water molecule and to enhance the electrophilic character of the substrate. Other notable members of this family of proteins include phosphotriesterase and urease, among others (*9*, *10*). The recent high-resolution X-ray structural analysis of DHO unveiled the participation of six amino acids in the assembly of the binuclear metal center (*7*). Each of the two divalent cations is directly ligated to two histidine residues, while one of the metal ions is additionally coordinated to an aspartate residue. The two metal ions are bridged by a solvent hydroxide and a carbamate functional group formed from the posttranslational carboxylation of the ϵ-amino group of a lysine residue.

Here we describe the crystallization and high-resolution X-ray crystallographic analysis of IAD from *E. coli* in both the unbound state and complexed with L-aspartate. On the basis of ultracentrifugation and gel filtration experiments, IAD is an octamer. The three-dimensional fold of each subunit is dominated by a $(\beta/\alpha)_8$-barrel motif with a binuclear metal center located at the C-terminal end of the barrel. Unlike the structure of DHO, there is an additional N-terminal domain formed by Met 1 to Gly 63 and Gly 346 to Thr 389 in IAD. Indeed, the two-domain structure of IAD is reminiscent to that observed for urease (*10*). Ligands to the metals in IAD include His 68, His 70, His 201, His 230, and Asp 285. The two metals are bridged by a carboxylated lysine residue (Lys 162) and a solvent molecule. This structural analysis defines both the quaternary structure of the enzyme and the active site geometry and confirms that, indeed, IAD belongs to the urease-related amidohydrolase superfamily (*6*).

MATERIALS AND METHODS

Protein Purification. For expression of the IAD protein, the *iadA* gene from *E. coli* was amplified by PCR with two primers, 5′-GGAATTCCATATGATTGATTATACCGCAG-CCGG-3′ and 5′-GGCGAATTCTCATCATCATCATTAA-GCCG-3′, containing *NdeI* and *EcoRI* sites, respectively. The resulting fragment was inserted into the *NdeI* and *EcoRI* sites of a pET30 plasmid. The protein was expressed in the strain BL21(DE3)star (Novagen). Cultures were grown in Luria−Bertani medium at 37 °C with a rotatory shaker until an A_{600} of ∼0.5−0.7 was reached. Induction was initiated by the addition of 1.0 mM isopropyl-β-thiogalactoside (IPTG), and the culture was further incubated overnight. The bacterial cells were isolated by centrifugation at 4500 × *g* for 15 min at 4 °C. The pellet was re-suspended in 5.0 mL of 50 mM Tris-HCl buffer, pH 8.1 (buffer A), 5 μg/mL of RNAse containing DNAse, and 0.1 mg/mL of the protease inhibitor (PMSF) per gram of cells and disrupted by sonication. The soluble fraction was separated from the lysed cells by centrifugation at 12 000 × *g* for 15 min at 4 °C. The protein solution was fractionated between 20% and 50% saturation of ammonium sulfate. Precipitated protein was resuspended in a minimum quantity of buffer A and loaded onto a ACA gel filtration column using 20 mM Tris, pH 8.1 (buffer B) as the elution buffer. Fractions that contained IAD were pooled and loaded onto a Resource Q ion exchange column and eluted with a gradient of NaCl in buffer B. The final step in the purification was accomplished with a Superdex 200 gel filtration column and elution with buffer A. The purity of IAD during the isolation procedure was monitored by SDS−PAGE. The concentration of the enzyme was determined by measuring the absorbance at 280 nm using an extinction coefficient of 18 307 M^{-1} cm^{-1}.

Enzyme Assays. The substrates, iso-Asp-Leu and iso-Asp-Gly, were purchased from Sigma. The coupled enzyme assay monitors the production of aspartate through conversion to oxaloacetate and malate by the action of aspartate aminotransferase and malate dehydrogenase. The assay mixtures contained 100 mM HEPES pH 8.0, 100 mM KCl, 3.7 mM α-ketoglutarate, 0.4 mM NADH (Calbiochem), 0.36 units malate dehydrogenase (Sigma), 6 units aspartate aminotransferase (Sigma), the appropriate dipeptide substrate, and IAD in a final volume of 250 μL. The oxidation of NADH at 30 °C was followed spectrophotometrically at 340 nm.

Molecular Weight Determination. Sedimentation velocity experiments were performed on a 2.0 mg/mL sample of IAD in 50 mM Tris-Cl buffer at pH 8.1. The experiments were performed with a Beckman Optima XL-A centrifuge and an An 60 Ti rotor at 25 °C. The 12 mm double sector charcoal-filled Epson centerpieces had a sample capacity of 300 μL, and experiments were conducted at a rotor speed of 42 000 rpm with scans at 4 min intervals. The sedimentation of IAD was monitored by the absorption of light at 280 nm. The sedimentation data were analyzed with the program SVEDBERG and gave an $s_{20,w}$ value of 12.9 S and a molecular weight of ∼320 000.

The molecular weight of IAD was also estimated using gel filtration. A HiLoad 16/60 Superdex 200 column (Pharmacia) was calibrated with six standard molecular weight markers (MW-GF-1000 from Sigma). IAD was applied to the column and eluted with buffer A at a flow rate of 1.0

Table 1: X-Ray Data Collection Statistics

data set	resolution (Å)	independent reflections	completeness (%)	redundancy	avg I/avg $\sigma(I)$	R_{sym}[a] (%)
native no. 1	30.0−1.95	69425	95.1	5.0	6.2	9.2
	2.04−1.95[b]	5648	82.2	1.7	1.6	26.7
mercury	30.0−2.70	26596	95.0	3.1	6.7	8.6
	2.82−2.70	2740	81.6	1.5	1.8	22.7
gold	30.0−2.70	26598	95.0	3.3	4.8	9.6
	2.82−2.70	2615	77.9	1.5	1.7	23.2
lead	30.0−2.70	26711	95.3	2.9	5.8	9.3
	2.82−2.70	2508	74.7	1.5	1.9	23.2
native no. 2	30.0−1.65	112776	98.2	9.2	13.9	7.6
	1.73−1.65	12288	81.8	4.0	2.3	34.7
IAD/Asp	30.0−2.10	55201	94.5	4.2	6.7	8.2
	2.20−2.10	5640	75.4	1.9	1.6	26.3

[a] $R_{sym} = (\Sigma|I - \bar{I}|\Sigma I) \times 100$. [b] Statistics for the highest resolution bin.

mL per minute. The protein eluted between α-amylase and apoferritin, and the molecular weight was calculated to be 316 000. Since the molecular weight of the monomeric species is 41 084, the protein apparently exists as an octamer in solution.

Crystallization of IAD. A search for crystallization conditions was conducted utilizing an "in-house" sparse matrix screen composed of 144 conditions at both room temperature and at 4 °C via the hanging drop method of vapor diffusion. The best crystals were observed growing at 25 °C from 10% poly(ethylene glycol) 8000 (PEG-8000), 100 mM homopipes (pH 5.0), and in the presence of $MgCl_2$. Large single crystals were subsequently obtained from hanging drops with precipitant solutions of 6−8% PEG-8000 buffered with 100 mM homopipes (pH 5.0) and containing 50−100 mM $MgCl_2$. The enzyme concentration was typically 11.0 mg/mL, and the protein solution was buffered in 50 mM Tris (pH 8.1). Crystals achieved maximum dimensions of 0.5 mm × 0.5 mm × 0.3 mm in approximately 1 week. They belonged to the space group $P42_12$ with unit cell dimensions of $a = b =$ 119.0 Å, and $c = 138.8$ Å and contained two subunits in the asymmetric unit.

Initial Structural Analysis of IAD. An initial X-ray data set was collected to 1.95 Å resolution at 4 °C with a Bruker HISTAR area detector system equipped with Supper "long" mirrors. The X-ray source was CuKα radiation from a Rigaku RU200 X-ray generator operated at 50 kV and 90 mA. The X-ray data were processed with XDS (*11*, *12*) and internally scaled with XSCALIBRE (Rayment and Wesenberg, unpublished). Relevant X-ray data collection statistics are presented in Table 1.

Three isomorphous heavy-atom derivatives were prepared by soaking native crystals in either 1 mM methylmercury acetate for 1 day, 5 mM gold(I) cyanide for 3 days, or 40 mM trimethyllead acetate for 2 days. The gold and mercury derivatives were obtained by first soaking the crystals in 1 mM iodoacetamide overnight at pH 6.0 (buffered with 100 mM homopipes) and then back-soaking in a synthetic mother liquor to remove any remaining iodoacetamide before heavy-metal derivatization at pH 6.0. The lead derivative was obtained without treating the crystals with iodoacetamide but rather by increasing the pH of the soaking solution to pH 7.0 (with 100 mM homopipes as the buffer) to facilitate the binding of the trimethyllead cations. X-ray data were collected for these heavy-atom derivatives to 2.7 Å resolution. The *R*-factors between the native and mercury, gold, and lead derivative data sets were 26.5%, 15.8%, and 17.0%, respectively (where $R = \Sigma|F_N - F_h|/\Sigma|F_N| \times 100$, F_N is the native structure factor amplitude, and F_h is the heavy-atom derivative structure factor amplitude). The locations of the heavy-atom binding sites (five, two, and three, respectively, per derivative) were determined with the software package SOLVE (*13*). The positions, occupancies, and temperature factors for these sites were refined with SOLVE yielding an overall figure-of-merit of 0.37 and phasing powers of 0.73, 0.54, and 0.47, respectively, for the three heavy-atom derivatives. Protein phases were calculated to 2.7 Å resolution with SOLVE. The rotational and translational matrices relating the two subunits in the asymmetric unit were determined with the program MUNCHKINS (*14*) based on the positions of the two gold cyanide binding sites. These matrices were employed for cyclical averaging with the solvent flattening software, DM (*15*), to give a figure-of-merit of 0.74 for the averaged electron density map. Approximately 95% of the amino acid residues were built into this initial "averaged" electron density map using TURBO (*16*). The model was then expanded back into the crystallographic unit cell and refined with TNT (*17*). The resulting electron density maps calculated with coefficients of the form $(2F_o - F_c)$ or $(F_o - F_c)$ at 1.95 Å resolution were then averaged with the program AVE in the RAVE suite of programs (*18*, *19*). These maps allowed for the placement of the remainder of the amino acid residues. Finally, the "averaged" model was expanded back into the unit cell and the least-squares refinement completed with TNT to 1.95 Å resolution.

High-Resolution X-Ray Data Collection and Least-Squares Refinement. IAD crystals were harvested from hanging drop experiments and equilibrated in a synthetic mother liquor composed of 15% PEG-8000, 75 mM $MgCl_2$, 50 mM NaCl, and 100 mM homopipes (pH 5.0). These crystals were serially transferred to a cryoprotectant solution containing 22% PEG-8000, 75 mM $MgCl_2$, 175 mM NaCl, 12.5% ethylene glycol, and 100 mM homopipes (pH 5.0), suspended in a loop of 20 μm nylon, and then flash-frozen in a stream of nitrogen gas. The unit cell dimensions changed to $a = b = 116.7$ Å and $c = 138.5$ Å upon cooling to 100 K. A native X-ray data set was collected to 1.65 Å resolution, processed with SAINT (Bruker AXS, Inc.), and scaled as previously described. The high-resolution structure of IAD was solved via molecular replacement with the program AMORE (*20*) and employing as the search model the X-ray coordinates

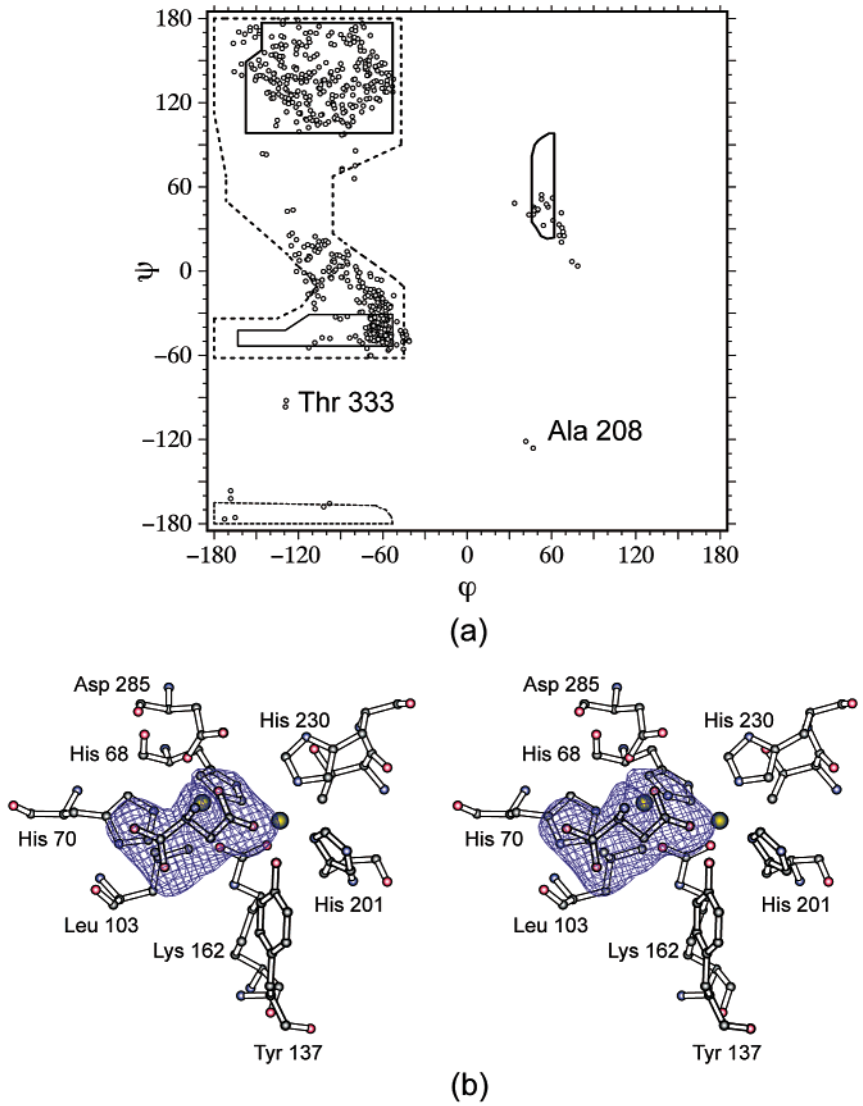

FIGURE 1: Quality of the X-ray model. Shown in panel a is a ϕ,ψ plot of all nonglycinyl residues for both subunits in the asymmetric unit (resting enzyme). Fully allowed ϕ,ψ values are enclosed by continuous lines; those only partially allowed are enclosed by broken lines. The electron density corresponding to the bound aspartate ligand in subunit II is displayed in panel b. The map was calculated with coefficients of the form $(F_o - F_c)$, where F_o was the structure factor amplitude from the "aspartate-soaked" crystals and F_c was the calculated structure factor amplitude from the model lacking the coordinates for the ligand. The map was contoured at 3σ.

derived at 1.95 Å resolution. Iterative cycles of least-squares refinement and manual model building reduced the *R*-factor to 18.2% for all measured X-ray data from 30.0 to 1.65 Å resolution. Relevant least-squares refinement statistics are given in Table 2, and a Ramachandran plot of all nonglycinyl residues is presented in Figure 1a. There are only two significant outliers in each of the molecules contained within the asymmetric unit: Ala 208 and Thr 333. The electron density corresponding to these residues is unambiguous. Ala 208 is situated at the end of a type III turn, while Thr 333 is located at the end of a type I turn which leads into an α-helix. The *E. coli* IAD contains 390 amino acid residues. In the crystal structure, the polypeptide chain for subunit I extends from Met 1 to Thr 389 with only a break between Ser 289 and Gly 303, while for subunit II, the polypeptide chain extends from Met 1 to Thr 389 with a break between Pro 291 and His 301.

X-ray Data Collection and Least-Squares Refinement of IAD Complexed with L-Aspartate. IAD crystals were harvested from hanging drop experiments and equilibrated in the same synthetic mother liquor as described above with

Table 2: Relevant Refinement Statistics

complex	native−resting	IAD/Asp complex
resolution limits (Å)	30.0−1.65	30.0−2.1
R-factor[a] (overall) %/ no. reflections	18.2/112728	18.2/55201
R-factor (working) %/ no. reflections	17.8/101398	17.7/49618
R-factor (free) %/ no. reflections	21.9/11330	24.6/ 5583
no. protein atoms	5620[b]	5620[c]
no. heteroatoms	773[d]	283[e]
bond lengths (Å)	0.014	0.013
bond angles (deg)	2.45	2.30
trigonal planes (Å)	0.006	0.008
general planes (Å)	0.015	0.012
torsional angles (deg)[f]	20.5	17.1

[a] *R*-factor $= (\Sigma|F_o - F_c|/\Sigma|F_o|) \times 100$, where F_o is the observed structure-factor amplitude and F_c is the calculated structure-factor amplitude. [b] These include multiple conformations for Ser 56, Val 87, Val 100, Arg 364, and Glu 126 in subunit I and Ser 40, Val 87, Thr 120, Glu 126, Glu 239, and Asn 341 in subunit II. [c] These include multiple conformations for Asn 341 in subunit I and Asn 341 in subunit II. [d] These include four zinc ions, one magnesium ion, one sodium ion, three chloride ions, three ethylene glycol molecules, and 752 waters. [e] These include four zinc ions, two aspartates, and 261 waters. [f] The torsional angles were not restrained during the refinement.

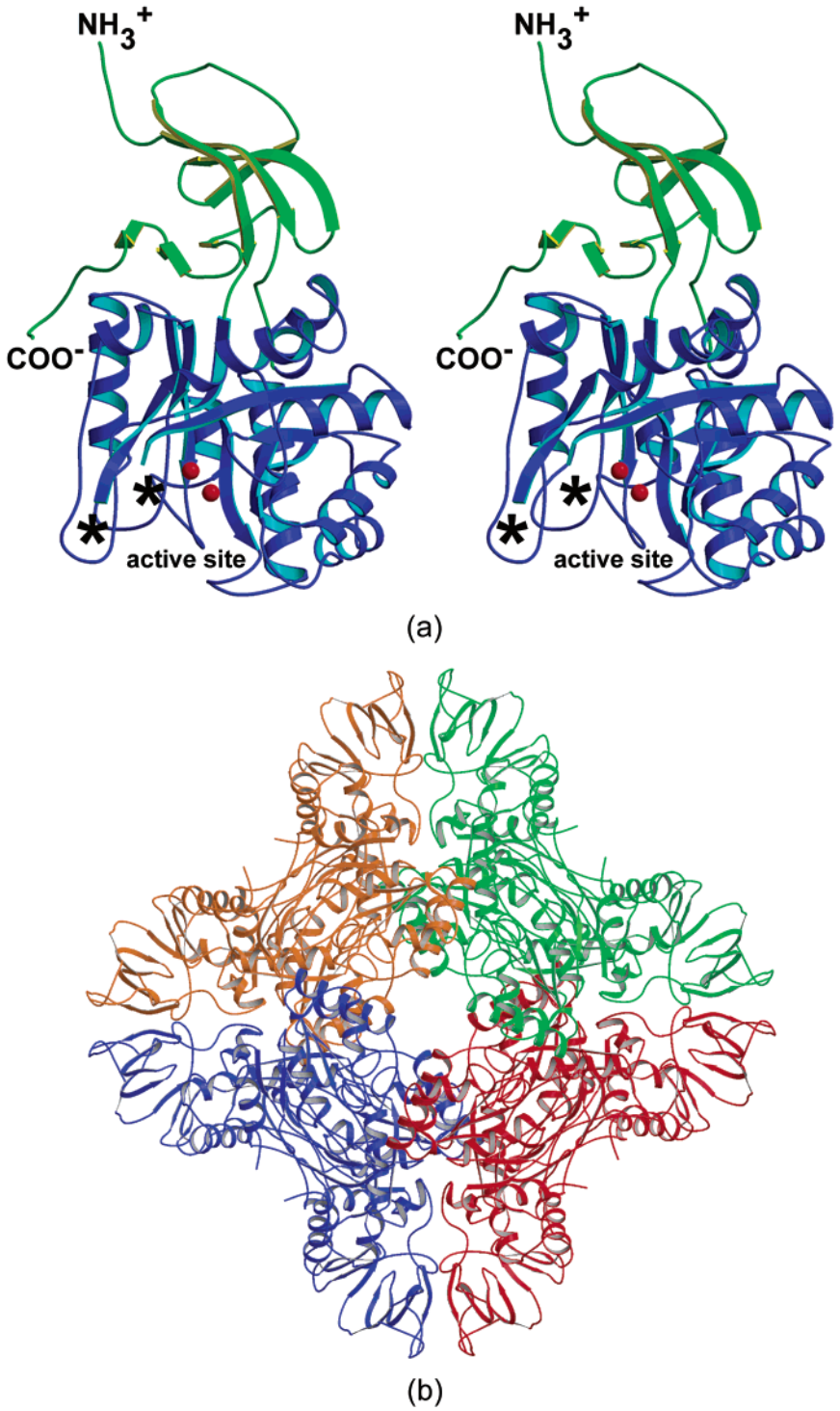

FIGURE 2: Quaternary and tertiary structure of IAD (resting enzyme). A ribbon representation of a single subunit of IAD is displayed in panel a. The N-terminal domain is colored in green while the $(\beta,\alpha)_8$ barrel, which constitutes most of the C-terminal domain, is depicted in blue. The positions of the two zincs are indicated by the red spheres. There is a break in the course of the polypeptide chain as indicated by the asterisks. The quaternary structure of IAD is shown in panel b. The molecule displays 422 symmetry and can be described as a tetramer of dimers. The four dimers are color-coded in red, green, blue, and gold.

the addition of 100 mM L-aspartate. An X-ray data set was collected to 2.1 Å resolution at 4 °C, processed with XDS (*11*, *12*), and scaled as previously described. The structure was solved via Difference Fourier techniques and refined with TNT. Relevant least-squares refinement statistics are given in Table 2. Electron density corresponding to the bound aspartate in subunit II is presented in Figure 1b. As can be seen, the electron density is well-ordered. In contrast to that observed for the unbound form of the enzyme, in the complex of IAD with L-aspartate, the loop defined by Ser 289 to Gly 303 was visible in the electron density maps for both molecules in the asymmetric unit.

RESULTS AND DISCUSSION

Tertiary Structure of the IAD Subunit (Unbound Form). The crystals employed in this investigation contained two subunits per asymmetric unit. For the sake of simplicity, the following discussion will only refer to subunit II of the

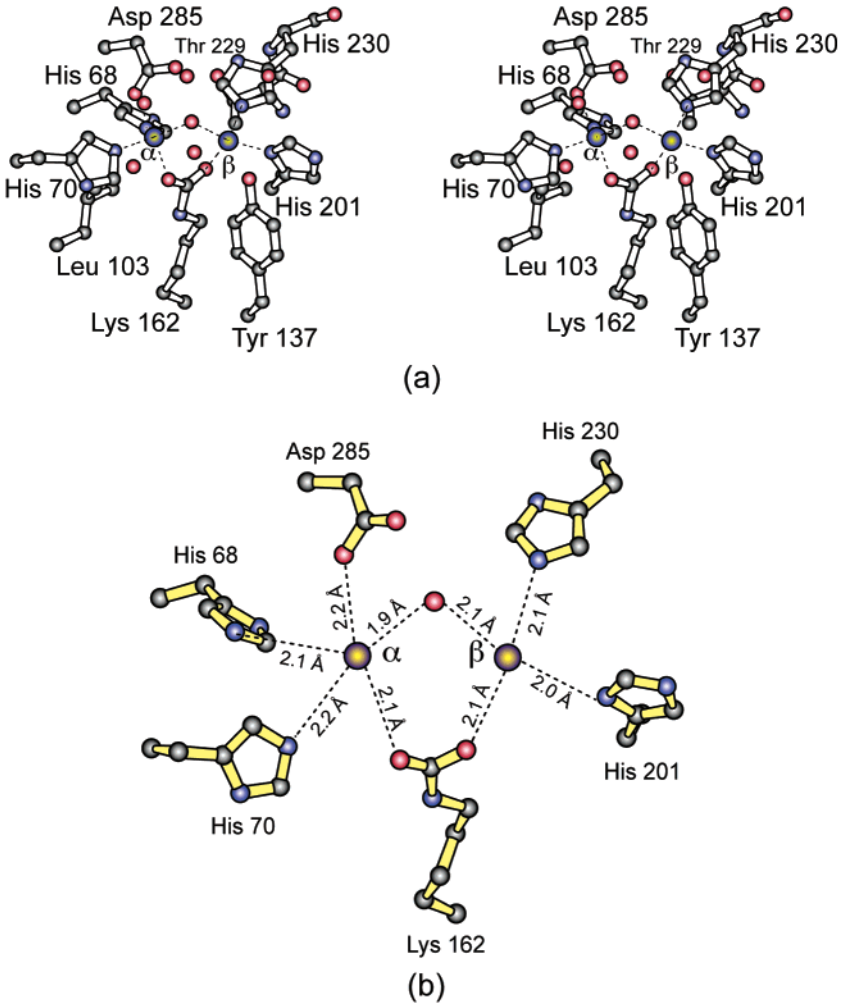

FIGURE 3: Active site of the resting enzyme. A close-up view of the active site near the binuclear metal center is displayed in panel a. The red spheres represent ordered water molecules. A schematic of the coordination geometry surrounding the binuclear metal center is given in panel b.

coordinate file. Note, however, that the two subunits in the asymmetric unit are virtually identical such that their α-carbons or all atoms superimpose with root-mean-square deviations of 0.26 and 0.51 Å, respectively. As shown in Figure 2a, the structure of the subunit is divided into two regions, with Met 1 to Gly 63 and Gly 346 to Thr 389 forming the N-terminal domain and Phe 64 to Lys 345-folding into a $(\beta/\alpha)_8$ TIM-barrel motif. The subunit is roughly globular with overall dimensions of approximately 60 Å × 55 Å × 55 Å. The N-terminal domain is characterized by an eight-stranded mixed β-sheet formed by Phe 9 to Tyr 18, Glu 21 to Val 30, Ile 35 to Ala 39, Thr 51 to Asp 54, Ile 59 to Val 62, Asp 355 to Met 359, Arg 364 to Tyr 369, and Leu 374 to Val 376. The eight strands forming the TIM-barrel motif are delineated by Phe 64 to Val 69, Val 97 to Leu 103, Ile 128 to Thr 134, Ile 159 to Ile 165, Val 197 to Met 202, Leu 226 to Thr 229, Ile 251 to Ile 253, and Val 280 to Ser 291. There is an additional β-strand defined by Ile 302 to Phe 307 that occurs after the break in the polypeptide chain backbone and leads back into the N-terminal domain. The β-strands of the TIM-barrel are connected to one another by 10 α-helices and a variety of reverse turns.

Interestingly, IAD contains three cis-prolines at positions 20, 140, and 260. Cis-proline 20 is located at the start of the second β-strand in the N-terminal domain. Pro 140 is positioned in a random coil region lying between β-strand 3 of the TIM-barrel and the connecting α-helix and is ~17 Å from the active site region. Likewise, Pro 260 is situated at ~16 Å from the active site but on the opposite side of the barrel opening. Pro 260 lies within the random coil region linking β-strand 7 of the TIM-barrel to the connecting α-helix. There is a break in the polypeptide chain backbone from Pro 291 to His 301, which connects the eighth β-strand of the TIM-barrel to the following ninth β-strand of the C-terminal domain. This break is ~11 Å from the binuclear metal center.

Quaternary Structure of the Octamer. Previous reports have indicated that the *E. coli* IAD has a molecular weight of 120 000 (*3*). Ultracentrifugation and gel filtration experiments, however, have indicated that the enzyme is, in fact, an octamer with an overall molecular weight of ~320 000. Examination of the molecular packing arrangement within the crystalline lattice reveals that the octamer is situated along the crystallographic 4-fold rotational axis, thereby resulting in only two subunits per asymmetric unit. A ribbon representation of the octamer, which can be likened to a Celtic cross, is shown in Figure 2b. It can be aptly described as a somewhat flattened "tetramer of dimers" displaying 422 symmetry. There is additional 2-fold rotational symmetry

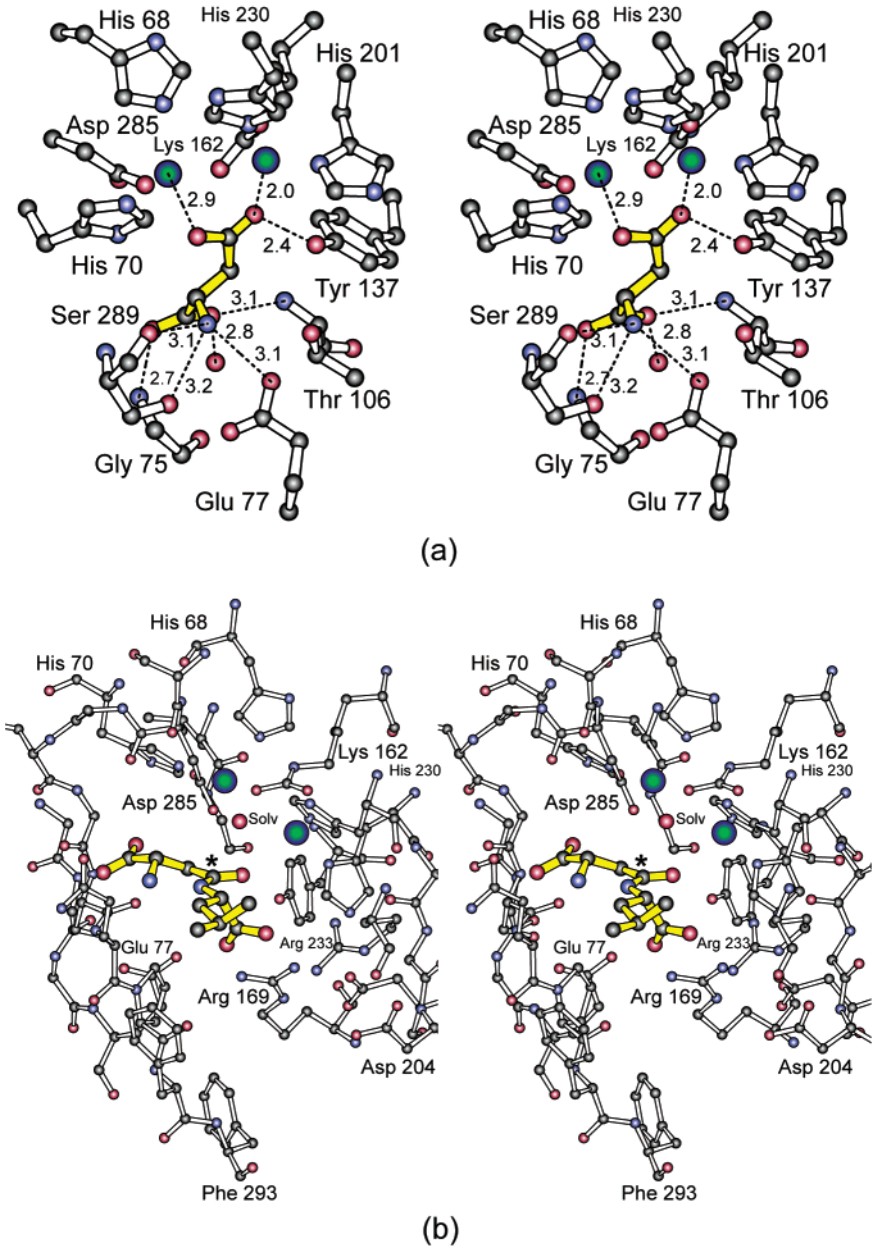

FIGURE 4: The active site with bound ligand. A close-up view of the active site with bound aspartate is displayed in panel a. Potential hydrogen bonding interactions are indicated by the dashed lines, and distances are given in ångströms. The ligand is highlighted in yellow bonds, and the zincs are depicted as green-blue spheres. A possible model for iso-Asp-Leu binding in IAD is shown in panel b. The iso-dipeptide is highlighted in yellow bonds. The position of the carbonyl carbon that is attacked during catalysis is indicated by the asterisk.

within each dimer. The overall dimensions of the octamer are ~130 Å × 130 Å × 80 Å, and the total surface area buried per subunit in the octamer is extensive at ~4400 Å^2. The two active sites within each dimer are separated by ~33 Å.

The Active Site. A close-up view of the active site of IAD without bound ligand is displayed in Figure 3a and a schematic of the coordination geometry for the binuclear zinc center is presented in Figure 3b. The two zinc cations are separated by 3.4 Å. As can be seen, the metals are bridged by a carboxylated lysine residue (Lys 162) and a solvent molecule, most likely a hydroxide ion. The more buried zinc ion, referred to as the α-metal, is coordinated by $N^{\epsilon 2}$ of His 68, $N^{\epsilon 2}$ of His 70, $O^{\delta 1}$ of Asp 285, O^2 of Lys 162, and the bridging hydroxide ion in a distorted trigonal bipyramidal arrangement. Asp 285 and Lys 162 serve as the axial ligands. Bond angles between an axial ligand, the zinc, and a equatorial ligand range from 83° to 98°. The second or β-metal of the binuclear zinc center is ligated by $N^{\delta 1}$ of His 201, $N^{\epsilon 2}$ of His 230, O^1 of Lys 162, and the bridging hydroxide ion in a quite distorted tetrahedral arrangement where the bond angles range from 89° to 112°.

Strikingly, O^{η} of Tyr 137 is located at 3.4 Å from the β-metal and in the proper position to serve as a fifth ligand in a trigonal bipyramidal coordination sphere. In this regard, the structurally equivalent β-zinc ion in phosphotriesterase is coordinated by five ligands in a distorted trigonal bipyramidal ligation sphere when diisopropyl methyl phosphonate, a sarin mimic, is bound in the active site (*21*). Indeed, the phosphoryl oxygen of the diisopropyl methyl phosphonate inhibitor occupies a somewhat similar position in the phosphotriesterase active site as that of O^{η} of Tyr 137 in

IAD. Note that Tyr 137 lies at the end of the third β-strand in the TIM-barrel. Inspection of the active site of dihydroorotase (DHO) shows that there is also a tyrosine residue (Tyr 104) in the same general position within the active site. However, due to changes in the polypeptide chain backbone beginning near Tyr 79 in DHO, this tyrosine residue resides at the end of the fourth β-strand of the TIM-barrel.

Structure of IAD with Bound Aspartate. The overall molecular fold of IAD with bound aspartate is essentially identical to that of the resting enzyme with the exception of the loop defined by Phe 292 to His 301. In the resting enzyme structure, the area of electron density corresponding to this region of polypeptide chain was too weak to model with confidence. Due to the interactions in the enzyme/aspartate complex between the α-amino group of the ligand and Ser 289, however, these residues become ordered. The α-carbon of Ser 289 moves by approximately 1.7 Å upon ligand binding. In the enzyme/aspartate complex, residues Gln 290 to Phe 293 serve as a continuation of the eighth β-strand of the TIM-barrel, residues Asp 294 to Gly 297 form a distorted type I′ turn, and residues Asn 298 to His 301 begin the ninth β-strand of the C-terminal domain. The only significant differences between the unbound and bound forms of the enzyme are limited to this region. Excluding these residues, however, the α-carbons for these two models superimpose with a root-mean-square deviation of 0.30 Å.

The observed hydrogen bonding pattern observed between the aspartate ligand and the protein is depicted in Figure 4a. The side chain carboxylate group of aspartate is wedged between the binuclear metal center with oxygen:α-metal and oxygen:β-metal distances of 2.9 and 2.0 Å, respectively. The oxygen that is coordinated to the β-metal is also located within 2.4 Å of O^{η} of Tyr 137. In DHO, there is a striking salt bridge between the α-carboxylate group of the *N*-carbamoyl aspartate substrate and the guanidinium group of Arg 20. In IAD, this interaction is replaced with the peptidic NH of Gly 75, and indeed, the backbone of IAD in this region superimposes with the side chain of Arg 20 in DHO. The α-carboxylate group of aspartate in IAD forms an additional hydrogen bonding interaction with the peptidic NH group of Thr 106 and a water molecule. As indicated in Figure 4a, the α-amino group of the ligand lies within hydrogen bonding distance to the side chains of Ser 289 and Glu 77 and the carbonyl oxygen of Ser 289.

Possible Substrate Binding Mode. As expected from amino acid sequence alignments, the overall three-dimensional structure of IAD is similar to that observed for DHO, phosphotriesterase, and urease (*7*, *9*, *10*). Unlike DHO and phosphotriesterase whereby the TIM-barrel constitutes the entire fold of the enzyme, IAD is more similar to urease with the additional N-terminal domain. Indeed, the α-carbons for IAD and urease superimpose with a root-mean-square deviation of 3.2 Å for 298 structurally equivalent amino acids. In all of these enzymes, the binuclear metal centers are similar with respect to metal:bond distances, metal:bond angles, and coordination geometries. The manner in which aspartate is accommodated within the active site of IAD as demonstrated here is reminiscent of that observed for *N*-carbamoyl aspartate in DHO. In both cases, the side chain carboxylate groups interact with the binuclear metal centers and displace the bridging hydroxides. In the structure of DHO complexed with dihydroorotate, the bridging hydroxide is

Scheme 3

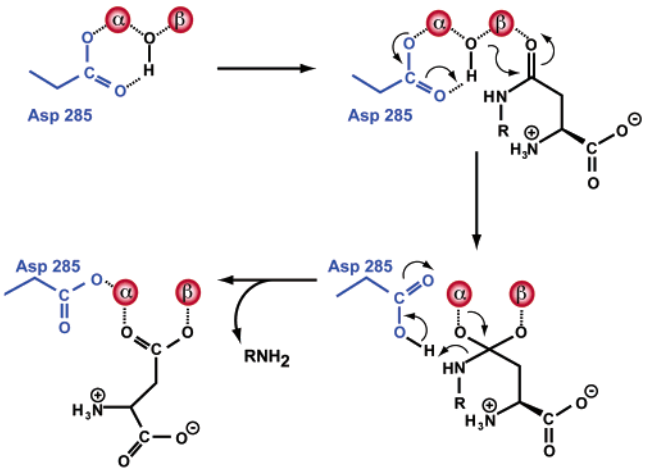

present, and O4 of dihydroorotate is located within 2.9 Å of the β-metal. Given these structures of DHO with bound product or substrate and the model of IAD with bound product, it is possible to speculate on the manner in which the isoaspartyl dipeptides might be accommodated in the IAD active site.

Shown in Figure 4b is a model of iso-Asp-Leu built into the IAD active site. This model was positioned into the active site by assuming that the α-carboxylate of the iso-Asp portion binds in the same manner as that observed for L-aspartate. The carbonyl oxygen of the peptide bond was positioned into IAD on the basis of the interactions observed between dihydroorotate and dihydroorotase (*7*). This model places the carbonyl oxygen within ~3 Å of the β-metal and 2.1 Å of Tyr 137 O^{η}. It is possible that the side chain of Tyr 137 shifts slightly in the active site upon iso-dipeptide binding. Using both the α-carboxylate group and the carbonyl oxygen as guide points, the modeling of the iso-dipeptide into the IAD active site results in the Leu moiety of the substrate being oriented toward the opening of the TIM-barrel (Figure 4b). There are two arginine residues in this region, namely Arg 169 and Arg 233, that may be important for proper substrate positioning by interacting with the carboxylate group of the Leu moiety. In light of this model and in keeping with what has been structurally observed for DHO, a possible reaction mechanism for IAD can be envisioned as outlined in Scheme 3. The bridging hydroxide ion of the binuclear metal center attacks the *re* face of the peptide carbonyl oxygen leading to a tetrahedral intermediate. This nucleophilic attack by the bridging hydroxide is assisted by general basis catalysis via Asp 285. The tetrahedral intermediate is stabilized through bidentate interactions with the α- and β-metals. Donation of the proton by Asp 285 to the peptidic nitrogen of the substrate leads to collapse of the intermediate and cleavage of the peptide bond. The only other possible candidates for proton donation to the leaving group include Glu 77, Tyr 137, or the α-amino group of the isoaspartyl moiety of the original dipeptide.

One question that can be raised is why iso-Asp-Leu is the best substrate for IAD and iso-Asp-Gly and iso-Asp-His are reportedly hydrolyzed very slowly. From this model, it is not possible to explain these data. Clearly a more complete picture of the molecular determinants for substrate specificity will emerge once the structure of the enzyme has been solved

in the presence of appropriate substrate analogues. These investigations are currently underway.

ACKNOWLEDGMENT

We thank Jungwook Kim for his determination of the molecular weight of IAD by ultracentrifugation. We are indebted to Leslie Dove and Tamiko M. Neal for the cloning of the *iadA* gene from *E. coli* into a suitable expression vector.

REFERENCES

1. Stephenson, R. C. and Clarke, S. (1989) *J. Biol. Chem. 264*, 6164−6170.
2. Fu, J. C., Ding, L., and Clarke, S. (1991) *J. Biol. Chem. 266*, 14562−14572.
3. Haley, E. E. (1968) *J. Biol. Chem. 243*, 5748−5752.
4. Gary, J. D. and Clarke, S. (1995) *J. Biol. Chem. 270*, 4076−4087.
5. Hejazi, M., Piotukh, K., Mattow, J., Deutzmann, R., Volkmer-Engert, R., and Lockau, W. (2002) *Biochem. J. 364*, 129−136.
6. Holm, L., Sander, C. (1997) *Proteins: Struct. Funct. Genet. 28*, 72−82.
7. Thoden, J. B., Phillips, G. N. Jr., Neal, T. M., Raushel, F. M., and Holden, H. M. (2001) *Biochemistry 40*, 6989−6997.
8. Cheon, Y. H., Kim, H. S., Han, K. H., Abendroth, J., Niefind, K., Schomburg, D., Wang, J., and Kim, Y. (2002) *Biochemistry 41*, 9410−9417.
9. Benning, M. M., Kuo, J. M., Raushel, F. M., and Holden, H. M. (1995) *Biochemistry 34*, 7973−7978.
10. Jabri, E., Carr, M. B., Hausinger, R. P., and Karplus, P. A. (1995) *Science 268*, 998−1004.
11. Kabsch, W. (1988a) *J. Appl. Crystallogr. 21*, 67−71.
12. Kabsch, W. (1988b) *J. Appl. Crystallogr. 21*, 916−924.
13. Terwilliger, T. C., and Berendzen, J. (1999) *Acta Crystallogr. D55*, 849−861.
14. Rypniewski, W. R., Breiter, D. R., Benning, M. M., Wesenberg, G., Oh, B.-H., Markley, J. L., Rayment, I., and Holden, H. M. (1991) *Biochemistry 30*, 4126−4131.
15. Cowtan, K., and Main, P. (1998) *Acta Crystallogr. D54*, 487−493.
16. Roussel, A., Fontecilla-Camps, J. C., and Cambillau, C. (1990) *Acta Crystallogr. A4*, C66−C67.
17. Tronrud, D. E., Ten Eyck, L. F., and Matthews, B. W. (1987) *Acta Crystallogr. A43*, 489−501.
18. Jones, T. A. (1992) in *Molecular Replacement* (Dodson, E. J., Gover, S., and Wolf, W., Eds.) SERC Daresbury Laboratory, Warrington, U.K., pp 91−105.
19. Kleywegt, G. J., and Jones, T. A. (1994) in *From First Map to Final Model* (Bailey, S., Hubbard, R., and Waller, D., Eds.) SERC Daresbury Laboratory, Warrington, U.K., pp 59−66.
20. Navaza, J. (1994) *Acta Crystallogr. A50*, 157−163
21. Benning, M. M., Hong, S.-B., Raushel, F. M., and Holden, H. M. (2000) *J. Biol. Chem. 275*, 30556−30560.

BI034233P